Available online at www.sciencedirect.com
ScienceDirect
Engineering Fracture Mechanics 74 (2007) 1770–1792
Engineering Fracture Mechanics
www.elsevier.com/locate/engfracmech

Numerical simulations of specimen size and mismatch effects in ductile crack growth – Part I: Tearing resistance and crack growth paths

E. Østby [a,*], C. Thaulow [b], Z.L. Zhang [b]

[a] SINTEF Materials and Chemistry, Department of Applied Mechanics and Corrosion, N-7465, Trondheim, Norway
[b] Norwegian University of Science and Technology, N-7491, Trondheim, Norway

Received 21 September 2004; received in revised form 24 August 2006; accepted 6 September 2006
Available online 17 November 2006

Abstract

The Gurson–Tvergaard–Needleman (GTN) model has been used for detailed numerical simulations of the effects of specimen size and yield stress mismatch on ductile crack growth behaviour in two different finite specimen geometries. For deep cracked bending specimens the crack growth resistance, expressed through the far-field J, increases as the specimen size is reduced, most strongly seen in case of low hardening. An opposite effect can be seen to some extent for shallow cracked specimens loaded in tension for low and intermediate hardening. For the yield stress mismatch cases low hardening and bend loading are found to promote crack growth deviation away from the initial crack plane.
© 2006 Elsevier Ltd. All rights reserved.

Keywords: Gurson–Tvergaard–Needleman model; Ductile crack growth; Size effect; Mismatch; Crack growth deviation

1. Introduction

Ductile crack growth plays an important role in the analysis of the fracture behaviour of structures. The crack extension reduces the load-bearing ligament and will influence the capacity of the structure. Further, ductile crack growth may also change the local near-tip stress/strain fields and can promote the transition to unstable cleavage fracture. This latter effect is of importance for steels in the ductile to brittle transition region. At the microscopic level ductile crack growth in metals is the result of nucleation, growth and coalescence of microvoids. The process involving rapid void growth is driven by high stress triaxiality as demonstrated by McClintock [1] and Rice and Tracey [2]. Rice and Johnson [3] also pointed out the importance of finite plastic deformation in order to allow for void growth. Both high stress triaxiality and large plastic strains are found in front of the crack tip, focusing the process of void growth in the material volume close to this. The volume in which the major part of the void growth takes place is often referred to as the process

* Corresponding author. Tel.: +47 98230440; fax: +47 73592931.
E-mail address: Erling.Ostby@sintef.no (E. Østby).

0013-7944/$ - see front matter © 2006 Elsevier Ltd. All rights reserved.
doi:10.1016/j.engfracmech.2006.09.013

zone for ductile crack growth. The process zone size/shape, which controls the energy absorbed in the process, is important both with regard to the local fracture mechanism and the global behaviour of the structure. In fracture mechanics, materials resistance to ductile crack growth is often expressed through the $J - \Delta a$ curve. However, this curve does not represent a material parameter, but is dependent on the geometry. Thus, great effort has been made in order to get a better understanding of the local mechanisms controlling the crack growth and their relation to global parameters such as the specimen geometry.

Two different analysis techniques, the cohesive zone model and the use of damage mechanics material models, have received the most attention with regard to the numerical simulation of ductile crack growth in recent years. The cohesive zone model is based on a phenomenological description of the process leading to final material separation at micro level based on the work of Dugdale [4] and Barenblatt [5]. The basic ingredient in the model is the work, Γ_0, needed to reach this state, and is given by a potential which is a function of the displacement between the two material surfaces. Tvergaard and Hutchinson [6,7] have presented a thorough discussion on the use of such models for simulations of crack growth. Extensions of the model to take into account the effect of different constraint levels on the cohesive energy have also been proposed by Tvergaard and Hutchinson [8] and Siegmund and Brocks [9,10]. Considerable attention has also been given to the use of damage mechanics models for the simulation of ductile crack growth. The two most commonly used models are those of Gurson [11] and Rousselier [12], in which the effect of void growth is taken into account in the constitutive equations. The Gurson model has later been modified by Tvergaard and Needleman [31], thus, it is most often referred to as the Gurson–Tvergaard–Needleman (GTN) model. In addition to simulation of void growth the models can also be modified to take the effect of void nucleation and coalescence into account. Because the damage mechanics models represent constitutive material equations, the effect of different constraint levels is directly included in the analysis. However, incorporation of damage naturally leads to the inclusion of a material length scale linked to the element size in the model. A consequence of this is that results from numerical FE analyses tend to depend on the mesh size used. Examples of the application of damage mechanics to simulate crack growth can be found in Xia and Shih [13,14], Xia et al. [15], Ruggieri and Dodds [16], Gao et al. [17], and Zhang et al. [18] using the GTN model, and Burstow and Howard [19], using the Rousselier model. The relations between the cohesive zone and mechanism-based damage mechanics models have been discussed by several authors. In work with the computational cell by Xia and Shih [13,14] it is shown that a relation between the cohesive zone energy, Γ_0, and the element size, D, will take the form $\Gamma_0 \sim \sigma_0 \mathrm{D}$, where σ_0 is the yield stress of the material. Siegmund and Brocks [9,10,20] have compared the two different approaches and found quite a good correlation if the cohesive energy is calibrated from GTN model cell analysis and a dependency in the stress triaxiality is introduced. However, they argue that the two models are quite different with regard to how a length parameter is introduced. In the GTN model analysis the length parameter is related to the void spacing/microstructure of the , whereas in the cohesive zone model it is related to the critical displacement at the crack tip.

The fracture analysis of weldments is made more complex due to the inhomogeneous material properties. A mismatch in yield stress and/or work hardening between the base metal and weld metal is frequently encountered. This will influence the crack tip conditions for cracks located in the centre of the weldment and on the fusion line. For fusion line cracks, analyses show that the stress level in the weakest material is higher compared to what is found in the homogeneous material, Thaulow et al. [21]. This difference in stress field may have profound effects on the resistance to the initiation of cleavage fracture and ductile crack growth. Further, the asymmetrical stress/strain distribution may also cause deviation in the crack growth path in the case of cracks located close to the fusion line.

The main body of work on the simulation of ductile crack growth has been on homogenous material. For simulation of crack growth along the interface in bi-material specimens, most results stem from the use of the cohesive zone model, see e.g. Tvergaard and Hutchinson [22], Lin et al. [23]. Proposals for modelling of arbitrary crack paths using cohesive elements have been reported by Xu and Needleman [24] and Scheider [25]. Burstow and Howard [26] used the Rousselier model to simulate the effect of mismatch for cracks lying in the centre of weldments. They found that mismatch between the weld metal and the base metal could have a significant effect on the crack growth resistance. Similar results were found by Moran and Shih [27] using the GTN model. In these analyses a symmetrical situation was considered, and thus no change in crack growth path was to be expected. Hao et al. [28] used the GTN model to simulate crack growth starting at interfaces between materials

with different plastic properties. Their results showed that mismatch in general decreased the crack growth resistance in terms of the $J - \Delta a$ curve and the level of reduction was dependent on the mismatch.

In this paper we focus on two aspects related to ductile crack growth: The effect of specimen size for homogeneous materials, and the effect of mismatch in yield stress for interface cracks in bi-materials. Two finite geometries with different constraint levels are used in the study.

Section 3 discusses the effect of specimen size for different assumptions of hardening. Section 4 contains a discussion on the major new aspects related to ductile crack growth in bi-materials with differences in plastic properties. The results from the simulations of ductile crack growth in the bi-material specimens are presented in Section 5. The effects of ductile crack growth and mismatch on the near tip stress fields and the possible transition to cleavage fracture are discussed in Part II of the paper.

2. Numerical procedures

2.1. Specimen geometries

In this work we study the crack growth behaviour in two different finite geometries. The first geometry is a shallow cracked specimen, with relative crack depth $a/W = 0.15$, loaded in tension. The loading is applied by prescribing a uniform displacement, thus, the loading corresponds to a clamped boundary condition with regard to rotation at the ends. The second geometry is a deep cracked specimen, with relative crack depth $a/W = 0.5$, loaded in bending. The two geometries with definition of relevant dimensions are shown in Fig. 1. The length of the specimens, S, is chosen to be four times the thickness, W, in all the analyses. As seen from Fig. 1, the specimens are represented as bi-materials, with Mat 1 and Mat 2 having different material properties in the case of mismatch. The choice of the two different geometries is made in order to evaluate the effect of different constraint levels. The effect of specimen size is studied by considering geometrically similar specimens with different absolute size. Four different specimen sizes are used both for the tensile and the bend specimen: $W = 25$, 50, 100 and 200 mm. In the text W will be used when referring to the specimen size.

2.2. Materials

Referring to Fig. 1, the mismatch ratio between Mat 1 and Mat 2 is defined as:

$$m = \frac{\sigma_{0,2}}{\sigma_{0,1}} \tag{1}$$

where $\sigma_{0,1}$ and $\sigma_{0,2}$ are the yield stress of Mat 1 and 2, respectively. Mat 1, the material in which crack growth takes place, is modelled as a GTN material and Mat 2 is modelled as a classical von Mises material.

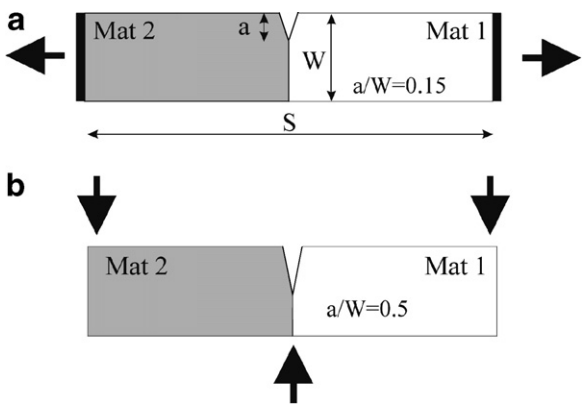

Fig. 1. The two finite geometries used in the present study. (a) Shallow cracked specimen, $a/W = 0.15$, loaded in tension. (b) Deep cracked specimen, a/W=0.5, loaded in bending.

The Poisson ratio is taken as $\nu = 0.3$. The relation between plastic strain and the flow stress used for Mat 2 and the matrix of Mat 1 is in the form:

$$\bar{\sigma} = \sigma_0 \left(1 + \frac{\varepsilon_p}{\varepsilon_0}\right)^n \tag{2}$$

where $\bar{\sigma}$ is the flow stress, σ_0 is the yield stress, ε_p is the equivalent plastic strain, $\varepsilon_0 = \sigma_0/E$ is the strain at yield, and n is the hardening exponent. A fixed ratio of $E/\sigma_0 = 500$, with $\sigma_0 = 400$, is used for Mat 1 in all the analyses. No mismatch in elastic properties between Mat 1 and Mat 2 is assumed. The yield function of the Gurson model has the following form:

$$\phi(q, \bar{\sigma}, f, \sigma_m) = \frac{q^2}{\bar{\sigma}^2} + 2q_1 f \cosh\left(\frac{3q_2\sigma_m}{2\bar{\sigma}}\right) - 1 - (q_1 f)^2 = 0 \tag{3}$$

where f is the void volume fraction, σ_m is the mean macroscopic stress, q is the conventional Mises stress, $\bar{\sigma}$ is the flow stress of the matrix material, and q_1 and q_2 are parameters introduced by Tvergaard [29,30]. Fixed values of $q_1 = 1.5$ and $q_2 = 1.0$ have been used in this study. Due to the incompressible nature of the matrix material the growth of existing voids can be expressed as:

$$\mathrm{d}f_{\mathrm{growth}} = (1 - f)\mathrm{d}\varepsilon^p : \mathbf{I} \tag{4}$$

where $\boldsymbol{\varepsilon}^p$ is the plastic strain tensor and $\mathbf{I}$ is the second-order unit tensor. In this work the increase in void volume fraction is assumed to be due solely to the growth of existing voids, and no void nucleation is introduced in the analysis. An initial void volume fraction of $f_0 = 0.002$ is assumed. Void coalescence after the material point has reached the critical void volume fraction, f_c, is numerically simulated by artificial acceleration of void growth as proposed by Tvergaard and Needleman [31]:

$$f^* = \begin{cases} f & \text{for } f \leqslant f_c \\ f_c + \frac{f_u^* - f_c}{f_F - f_c}(f - f_c) & \text{for } f > f_c \end{cases} \tag{5}$$

where $f_u^* = 1/q_1$. When $f > f_c$, f^* replaces f in (3). The critical void volume fraction, f_c, is evaluated according to Thomason's [32] plastic limit load criterion for transition from homogeneous deformation to localised deformation due to void coalescence. This criterion states that no coalescence will occur as long as the following condition is satisfied:

$$\frac{\sigma_1}{\bar{\sigma}} < \left(\alpha\left(\frac{1}{r} - 1\right)^2 + \frac{\beta}{\sqrt{r}}\right)(1 - \pi r^2) \tag{6}$$

Coalescence will first happen when the left-hand side becomes equal to the right-hand side in (6) In (6) σ_1 is the current maximum principal stress, r is the void space ratio defined as,

$$r = \sqrt[3]{(3f/4\pi)e^{\varepsilon_1+\varepsilon_2+\varepsilon_3}} / \sqrt{e^{\varepsilon_2+\varepsilon_3}/2} \tag{7}$$

and ε_1 is the maximum principal strain, ε_2 and ε_3 are the two other principal strains. For plane strain problems, (8) can be used with $\varepsilon_3 = 0$. In Thomason's original analysis, $\alpha = 0.1$ and $\beta = 1.2$ were used. Pardoen and Hutchinson [33] and Zhang et al. [18] have later used cell model analysis to study the effect of hardening and have found that a relation:

$$\alpha(n) = 0.12 + 1.68n \tag{8}$$

where n is the hardening exponent, improves the prediction of coalescence. This latter hardening dependent value of α has been used in the present work.

2.3. FE mesh

The FE analyses are performed using ABAQUS. Both Mat 1 and Mat 2 are modelled with fully integrated 4 node plane strain elements (ABAQUS type CPE4). Large deformation effects are accounted for in the analyses. Although it is not a general rule, the most commonly chosen mesh pattern for simulation of ductile crack

growth consists of a row of initially square shaped elements along the crack growth path. Also, most analyses assume a symmetrical loading condition and homogeneous material, thus only half of the specimen is modelled (with the element size corresponding to half the process zone height). When analysing cracks that are initially laying on the interface between two materials the symmetry assumption is no longer valid, and both sides have to be modelled. This introduces different constraint conditions for the elements along the interface compared to what is found for elements along a symmetry plane, and the element experiences constraint from both the materials on the top and on the bottom. A consequence of this is that a bending deformation is imposed on the element closest to the crack tip. Initial tests with quadratic shaped elements in the full model revealed strong oscillations in the near-tip stress field due to the additional constraint and the very fast void growth rate in the first element ahead of the crack tip caused significant numerical problems. Tests with elements allowing for incompatible mode deformation and reduced integration did not give any significant improvement in the results. However, results for elements with an aspect ratio equal to 2 (with the shortest element side parallel to the interface) displayed significantly more stable behaviour with regard to the

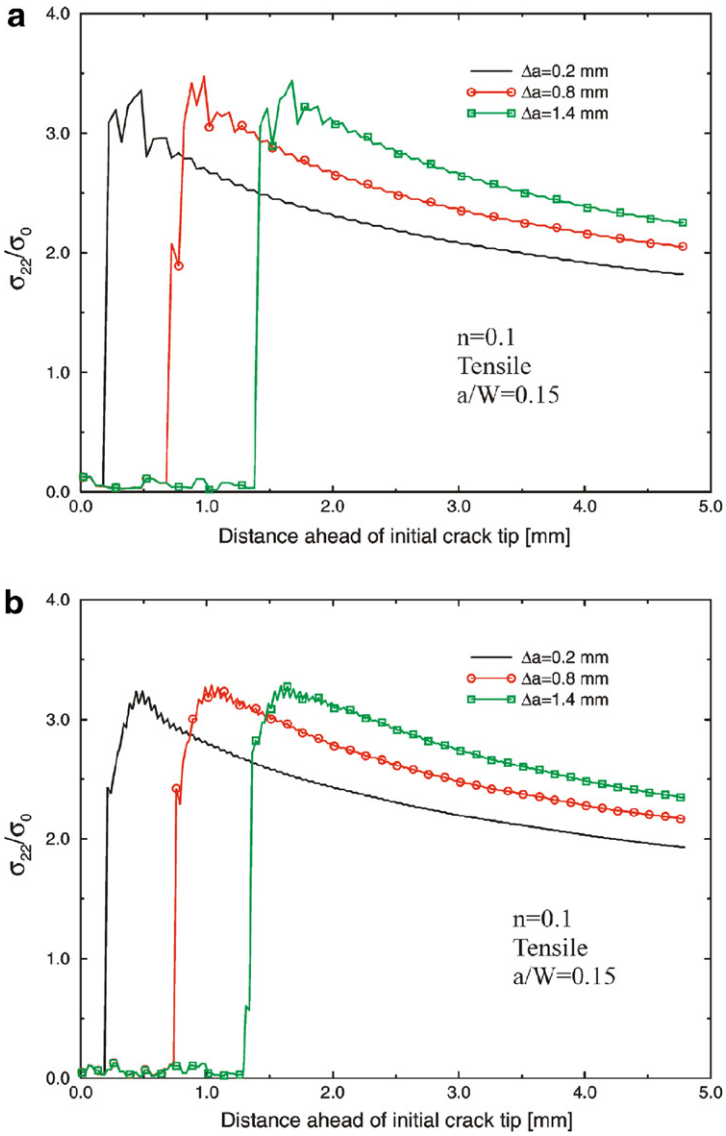

Fig. 2. Comparsion of resulting stress fields from initially square shaped elements and elements with aspect ratio 2. (a) Stress fields from square elements. (b) Stress fields from elements with aspect ratio 2.

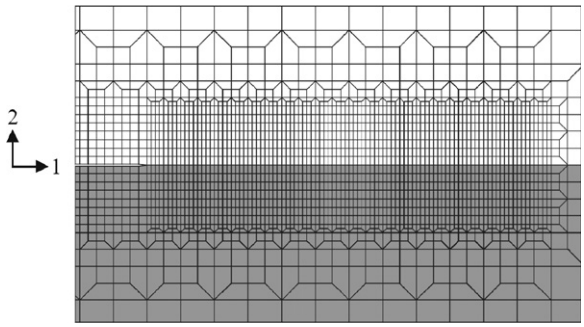

Fig. 3. Near tip details of the FE mesh used in the analyses. White area corresponds to Mat 1 (Gurson-material) and gray area corresponds to Mat 2 (Mises-material).

near-tip stress field and also gave less numerical problems. In Fig. 2 the stress fields resulting from use of initially square shaped elements and elements with aspect ratio 2, respectively, are compared. The stress fields are plotted for three different amounts of ductile tearing, Δa. These results were obtained using a specimen with $a/W = 0.15$ loaded in tension, with a hardening exponent $n = 0.1$ and a mismatch ratio $m = 1.5$ between Mat 2 and 1. The stress values are extracted in Mat 1 from the integration points closest to the interface between the two materials. The case with square elements is shown in Fig. 2(a). From this figure it can be observed that the opening stress just in front of the current crack tip displays some significant oscillations. This was judged not to represent a physical behaviour of the stress fields. Fig. 2(b) shows the same results, however, now with elements with an aspect ration of 2. In this case a much smoother stress field, with only very minor oscillations, is observed.

Due to the more stable numerical performance and the more well-behaved stress field, elements with an aspect ratio equal to 2 is used in all the analyses. The element size is $0.05 * 0.1$ mm. The region with uniform element size extends 4.8 mm ahead of the initial crack tip and 0.7 mm in each direction normal to the interface. Details of the near-tip mesh used are shown in Fig. 3.

2.4. Calculation of crack driving force parameter

In small scale yielding where proportional loading takes places, the J-integral will be independent of the choice of integration path. In the case of ductile crack growth path independence in the vicinity of the crack tip no longer exists due to the strong non-proportional loading in this area. However, J values evaluated on contours far away from the zone of highly non-proportional loading display more or less path independence. Good path independence was found for both specimen geometries and for the mismatch cases when using the far field J in the FE analyses, and all J values have been calculated according to the domain integral method implemented in ABAQUS.

3. HOMOGENEOUS MATERIAL – Effect of specimen size and hardening on ductile crack growth resistance

Three different hardening levels for the matrix material, $n = 0.05$, 0.1, and 0.2, are applied for both the low and high constraint geometry. Fig. 4(a)–(c) show the calculated $J - \Delta a$ curves for the low constraint tensile specimen. For the lowest hardening level, $n = 0.05$, in Fig. 4(a) it can be seen that there is only a weak dependence on the specimen size with regard to initiation of ductile crack growth and the effect of specimen size is small for crack growth up to 1–1.5 mm. At larger amounts of crack growth the curves for the two smallest specimens start to display lower crack growth resistance, with the most pronounced effect for the smallest specimen, $W = 25$ mm. The largest specimen $W = 200$ mm, however, remains slightly below the specimen with $W = 100$ mm in the crack growth range considered. The results for the case with $n = 0.1$ is shown in Fig. 4(b). They display similar behaviour as for $n = 0.05$, with the two smallest specimen sizes showing a reduction in crack growth resistance at larger amounts of crack growth. However, this effect is less significant compared

to the case with $n = 0.05$. For the highest hardening level, $n = 0.2$, a more uniform effect of specimen size, with increasing resistance for decreasing specimen size. At this level of hardening the smallest specimen reveals the highest resistance.

The results for the high constraint specimens are shown in Fig. 4(d)–(f). For $n = 0.05$, the crack growth resistance increases with decreasing specimen size. Again, the results for $n = 0.1$, is similar to $n = 0.05$, but with a smaller effect of the specimen size. This trend also continues for the highest hardening level, Fig. 4(f), but now only the smallest specimen size, $W = 25$ mm, displays a markedly higher crack growth resistance. With regard to the deep cracked bend specimens, Xia et al. [15] have reported similar findings for the effect of specimen size on the $J - \Delta a$ curve.

Siegmund and Brocks [9] have calculated the cohesive energy, Γ_0, in simulations using damage mechanics, by dividing the plastic dissipation in the element layer where crack growth takes place, by the crack growth rate. Their results show that initially Γ_0 depends strongly on the amount of crack growth. However, after some crack growth only a very little change is observed, and Γ_0 remains almost constant. In the analyses considered here this may be seen from the critical strain to fracture staying more or less constant after about 1 mm of crack growth. In this region an approximate expression for Γ_0 is of the form:

$$\Gamma_0 \approx \left(\int_0^{\varepsilon_f} (1 - f_0)\sigma_e \mathrm{d}\varepsilon_p \right) h_e \tag{9}$$

where ε_f is the equivalent plastic strain at final coalescence, f_0 is the initial void volume fraction, σ_e is the equivalent stress, ε_p is the equivalent plastic strain, and h_e is the initial height of the element. Eq. (9) is actually the plastic energy dissipated divided by the initial element length parallel to the crack plane. With knowledge of ε_f a closed form evaluation of (9) can be made by use of (2). The main approximation in (9) lies in that the plastic

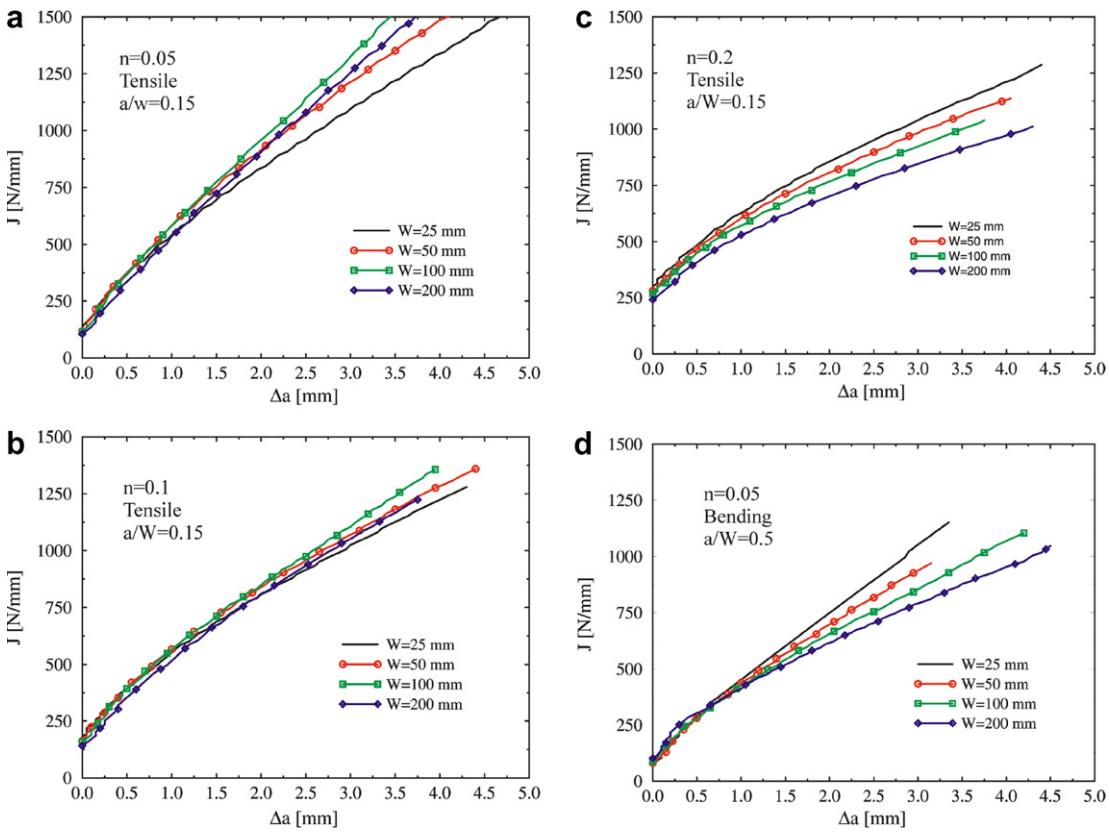

Fig. 4. The effect specimen size and hardening on the $J - \Delta a$ curves. (a)–(c) Shallow cracked specimens loaded in tension. (d)–(f) Deep cracked specimen loaded in bending (a) and (d) $n = 0.05$. (b) and (e) $n = 0.1$. (c) and (f) $n = 0.2$.

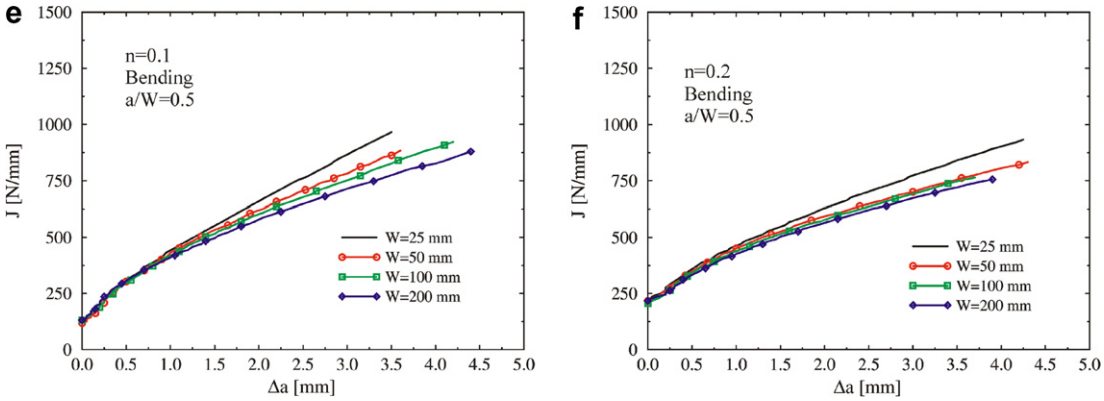

Fig. 4 (*continued*)

strain distribution ahead of the crack tip will change slightly with crack growth. However, the expression will serve our main purpose to discuss the influence of hardening on the local energy needed to sustain crack growth. The values of Γ_0 calculated from (9) for the three different hardening levels and the two different geometries, for the specimen size $W = 50$ mm, are shown in Table 1 together with ε_f. ε_f is extracted from the FE analysis as the strain value when the load carrying capacity in the element is reduced to zero.

From Table 1 it is noted that Γ_0 increases with increasing hardening for both geometries. Further, Γ_0 is higher in the tensile specimen compared to the bend specimen, as expected due to the lower stress triaxiality in the former geometry. With regard to the effect of hardening this observation is consistent with the results reported for crack growth simulations using a MBL model by Xia and Shih [13], where it was found that the crack growth resistance was increasing with increasing hardening. For the results in the finite geometry specimens shown in Fig. 4 it is noted that initiation occurs at a higher J for increasing hardening. However, contrary to the MBL results reported by Xia and Shih [13], the resistance at further crack growth in general decreases with increasing hardening. This difference appears to be due to the role played by the deformation in the remaining ligament. In the MBL model both deformation and stresses increase in an almost proportional way some distance away from the crack tip. In finite specimens significant ductile crack growth usually happens under conditions of fully plastic behaviour in the remaining ligament, and large plastic deformation extend to the back of the specimen. The necessary increase in deformation in the ligament is linked to the deformation needed to reach final fracture at the crack tip. From Table 1 it is seen that although the cohesive energy is higher for higher levels of hardening, the critical deformation, ε_f, increases with decreasing levels of hardening. Thus, the necessary increase in deformation in the remaining ligament to sustain crack growth is higher for lower levels of hardening.

The role played by the deformation in the remaining ligament can also explain the differences in the size effect observed in Fig. 4. In general the stress level ahead of the crack tip increases with increasing specimen size (see results in Part II of the paper). Thus from a local point of view a decrease in crack growth resistance should be expected for increasing specimen size. However, this does not hold true in general. Especially, for the tensile specimens with hardening $n = 0.05$, a drop in crack growth resistance is observed for the two smallest specimen sizes. Fig. 5(a) presents the plastic strain distribution ahead of the crack tip for the low constraint specimen. For growing cracks the farfield J does not scale the stress field in the same way as for stationary cracks. Thus, the

Table 1
Approximate values of cohesive energy, Γ_0, and the critical strain to fracture, ε_f, for different hardening and specimen geometries for specimen size $W = 50$ mm

n	Γ_0 (N/mm) (ε_f)	
	Tensile $a/W = 0.15$	Bending $a/W = 0.5$
0.05	20.5 (0.41)	15.3 (0.31)
0.1	21.4 (0.35)	16.8 (0.28)
0.2	27.5 (0.3)	23.2 (0.26)

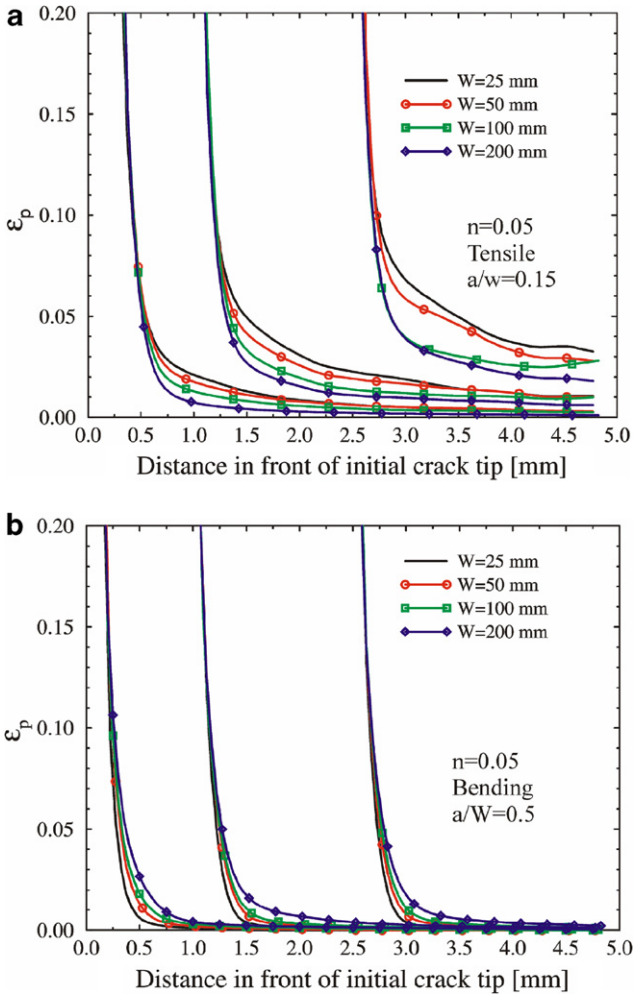

Fig. 5. Evolution of plastic strain ahead of the crack tip for different specimen sizes for the hardening level $n = 0.05$. (a) Shallow cracked specimen loaded in tension. (b) Deep cracked specimen loaded in bending.

stress fields can not be normalized. However, the resistance curves are only slightly dependent on the specimen size, thus the same Δa approximately corresponds to the J in the different specimens. It is seen that the general strain level increases both with decreasing specimen size and with crack growth for a given specimen size, indicating that the load in the remaining ligament increases with crack growth. Thus, strain localisation in the remaining ligament will happen more easily in the smaller specimens. This effect causes an overall smaller deformation in the remaining ligament necessary to drive the crack growth, and explains the drop in crack growth resistance in the smaller specimens. For the case with $n = 0.1$, Fig. 4(b), localisation of the deformation becomes less pronounced due to the higher level of hardening/more diffuse plastic deformation, and the drop in crack growth resistance for the smaller specimens is much less significant than for $n = 0.05$. Finally, for the highest hardening $n = 0.2$ in Fig. 4(c), the localisation of deformation is more difficult. The crack growth resistance is controlled by the increasing stress triaxialty in larger specimens, resulting in lower crack growth resistance for increasing specimen size. Thus, for tensile specimens the numerical simulations indicate that the nature of the size effect on crack growth resistance is dependent on the hardening level.

In the bending specimens the global deformation pattern is different compared to the tensile specimens (see Fig. 13). From Fig. 5(b) it is observed that the plastic strain level is decreasing with decreasing specimen size. In Fig. 4(d) it is seen that this, together with a higher stress level for increasing specimen size, results in a

decrease in crack growth resistance for larger specimens. The effect is also evident for the two other hardening levels, Fig. 4(e) and (f), but with decreasing effect of specimen size with increasing hardening. Thus, for the bending specimens, the nature of the size effect seems to be similar for all hardening levels investigated, but the importance of specimen size increases with decreasing hardening.

4. Mismatch

The results from the numerical simulation of ductile crack growth in mismatched specimens are reported in this section. As described in Section 2, the specimens are represented as bi-material specimens, with the crack initially lying on the interface between Mat 1 and Mat 2. Mat 1 is the material with the lower yield stress in which the ductile crack growth will take place. Three different mismatch levels, $m = 1.125$, 1.25, and 1.5, are

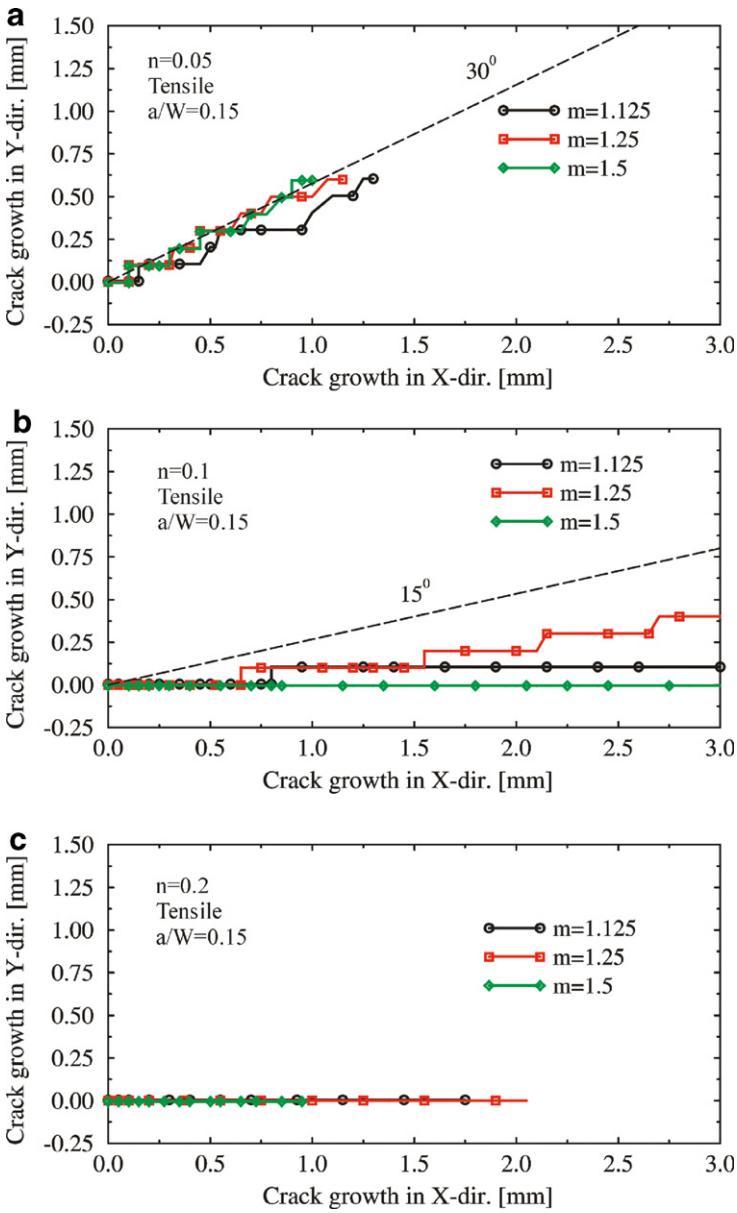

Fig. 6. The effect of specimen geometry, hardening, and mismatch level on the crack growth path. (a)–(c) Shallow cracked specimens leaded in tension. (d)–(f) Deep cracked specimens loaded in bending. (a) and (d) $n = 0.05$. (b) and (e) $n = 0.1$. (c) and (f) $n = 0.2$.

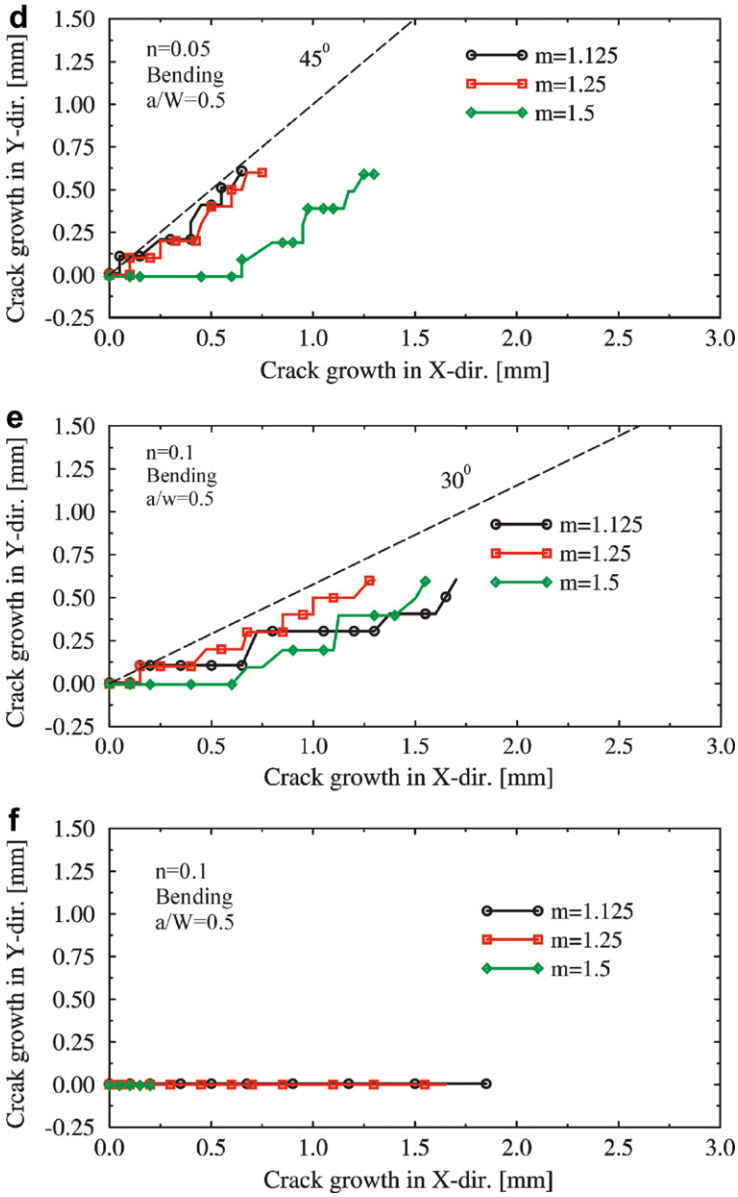

Fig. 6 (*continued*)

studied for the same specimen geometries and hardening levels used in Section 3. The specimen size is $W = 50$ mm.

4.1. Effect of mismatch on the crack growth path

Fig. 6 shows the crack growth paths for the different cases, with the x-direction parallel to the interface between the two materials. The crack growth paths for the three different mismatch levels for the tensile specimen with the lowest hardening, $n = 0.05$ are shown in Fig. 6(a). It can be seen that significant deviation from the interface takes place for all mismatch levels, with an average crack growth direction of about 30° to the interface. Fig. 6(b) shows the same result for the hardening level $n = 0.1$. Compared to the case with $n = 0.05$, a significantly lower tendency for crack deviation is observed. For the lowest mismatch level, $m = 1.125$, the crack grows about

0.5 mm along the interface, before it shifts to the second layer of elements and continues to grow here. The intermediate level of mismatch, $m = 1.25$, displays a stronger tendency towards deviation, but the crack grows along the interface for the highest mismatch level, $m = 1.5$. We see that some dependence on mismatch on the crack growth direction is found for this hardening level, but the average crack growth deviation is less than 10° for all levels of mismatch. For the case with $n = 0.2$, shown in Fig. 6(c) there is no crack growth deviation, and the crack grows along the interface for all mismatch levels. The crack growth paths in the bending specimen for the hardening level $n = 0.05$ are shown in Fig. 6(d). For the two lowest mismatch levels there is a very strong crack deviation, with an average crack growth angle of about 45° to the interface, is observed. For the highest mismatch level, $m = 1.5$, the crack initially follows the interface for about 0.5 mm, before a strong deviation also happens for this mismatch level. It is noted that the tendency towards crack growth deviation is stronger for the deep cracked specimen compared to what was found for the tensile specimen in Fig. 6(a). The results for the bend specimen with $n = 0.1$, Fig. 6(e), also display significant growth away from the interface. The tendency for larger deviation in the bend specimens compared to the tensile specimens, Fig. 6(b), is clearly evident for this hardening level as well. However, again it can be observed that for the highest mismatch level the crack grows along the interface initially for about 0.5 mm. As for the tensile case the crack growth in the bending specimens with the highest hardening level follow the interface between the two materials, as is shown in Fig. 6(f).

4.2. Effect of mismatch on the crack growth resistance

The effect of mismatch on the crack growth resistance is compared with the homogeneous case, $m = 1$, in this section. The crack growth, Δa, is defined as the projection of the actual crack growth path down on the interface between the two materials. The simulated $J - \Delta a$ curves are shown in Fig. 7. The results for the

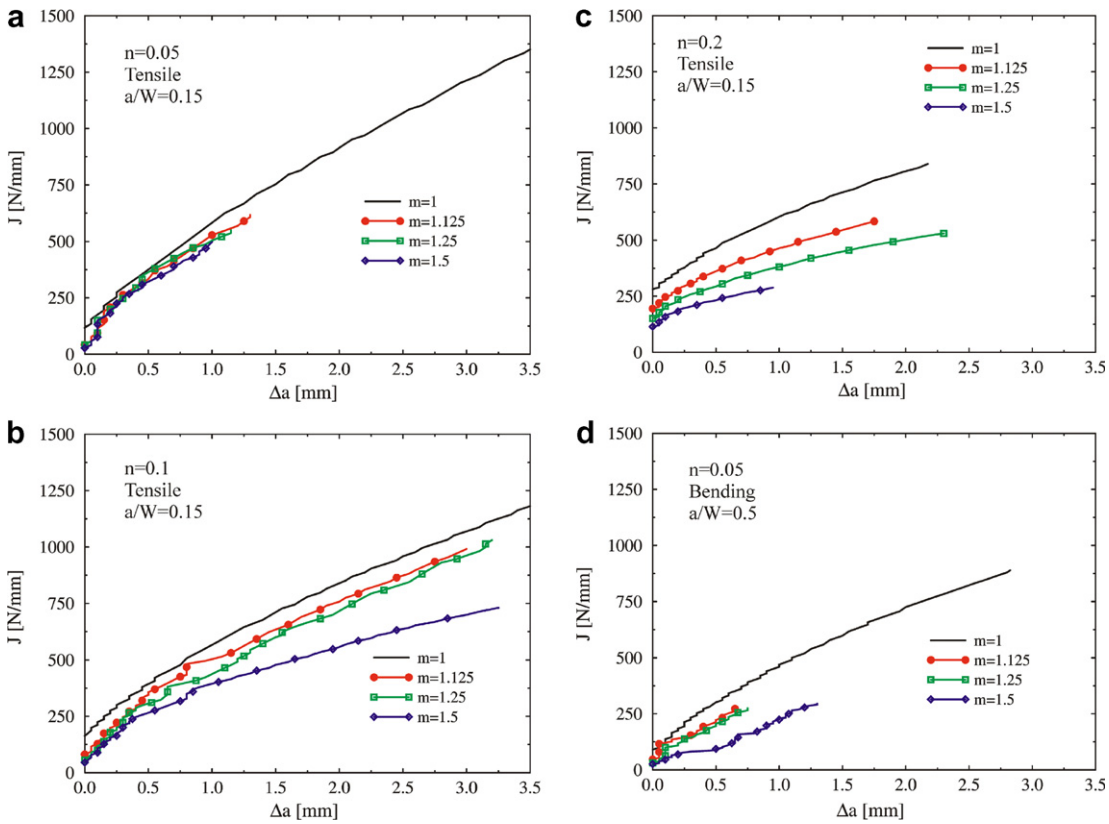

Fig. 7. The effect of specimen geometry, hardening, and mismatch level on the $J - \Delta a$ curves. (a)–(c) Shallow cracked specimens leaded in tension. (d)–(f) Deep cracked specimens loaded in bending. (a) and (d) $n = 0.05$. (b) and (e) $n = 0.1$. (c) and (f) $n = 0.2$.

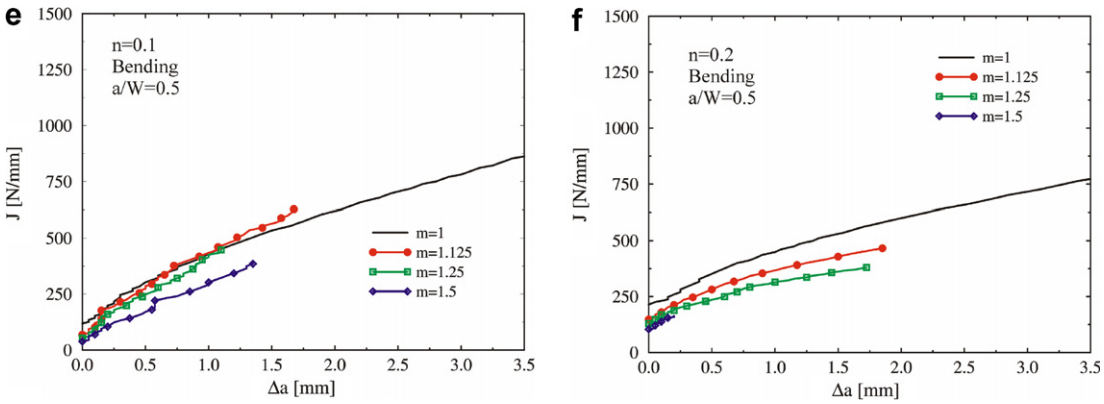

Fig. 7 (*continued*)

tensile specimen with hardening $n = 0.05$, Fig. 7(a) show that mismatch will slightly reduce the crack growth resistance, however the reduction is quite small. Further, the $J - \Delta a$ curves are almost the same for all three mismatch levels. This small effect of mismatch can be traced back to Fig. 6(a) where a significant crack growth deviation was observed. The amount of crack growth reported for the mismatch specimens is small because only the results while the crack tip is still inside the area of uniform mesh shown in Fig. 3 are included. Outside this area the results become strongly dependent on the changing element size. Fig. 7(b) shows the $J - \Delta a$ curves for the tensile specimen with $n = 0.1$. The two lowest mismatch levels only fall slightly below the curve for $m = 1$, but the slope of the curves is more or less similar to the homogeneous case. From Fig. 7(b) it was seen that the crack growth shifted away from the interface for these two mismatch levels, with the greatest tendency to deviation being for $m = 1.25$. For the highest mismatch level, $m = 1.5$, there is a significant reduction in the slope of the $J - \Delta a$ curves because the crack deviates away from the interface and the mismatch effect decreases. For the highest hardening level, $n = 0.2$, Fig. 7(c) shows a clear effect that the mismatch reduces the $J - \Delta a$ curve, with increasing reduction for increasing mismatch. As seen from Fig. 6(c) the crack growth path is along the interface for this hardening level. In Fig. 7(d) the results are shown for the bending specimens with $n = 0.05$. Only a very small amount of crack growth is reported for this specimen due to the fact that the crack grew rapidly out of the area with uniform mesh. A clearer effect of mismatch is seen initially here, even though very strong crack deviation was shown in Fig. 6(d). However, and not so easily seen from Fig. 7(d), the curves for both $m = 1.125$ and 1.25 have a slight upward curvature. This effect seems to be due to the tendency for the crack growth path to become crooked as shown more clearly in Fig. 14 for $m = 1.25$ (this result was obtained for a mesh with a larger area of uniform mesh size). For the highest mismatch level, $m = 1.5$, the initial part of the $J - \Delta a$ curve displays very little resistance to crack growth. This reason for this behaviour is discussed further in Section 4.4. Fig. 7(e) shows the $J - \Delta a$ curves for the bend specimen with $n = 0.1$. For the two lowest mismatch levels the slope is actually slightly higher than for the case with $m = 1$, resulting in an increasing resistance to crack growth for low levels of mismatch. This effect is similar to the slightly upward curvature noted for the case with $n = 0.05$. The curve for $m = 1.5$, however, falls below the curve for $m = 1$, mainly due to the initial part of crack growth along the interface seen in Fig. 6(e). Again, for the highest hardening level, $n = 0.2$, a significant reduction of the $J - \Delta a$ curve is seen in Fig. 7(f) due to the crack growth being along the interface.

4.3. Condition for crack growth deviation

The structure of the asymmetrical stress fields for mismatch cracks is complex, and a coupling between the radial and angular dependence of the stress components exists. Higher hydrostatic stresses, compared to the homogeneous case, exist in the weak material at some distance away from the interface and in front of the finite deformation zone the stronger material imposes an extra constraint on the plastic deformation in the weaker material at the interface. These two aspects will influence the damage evolution at an early stage,

promoting a higher rate of void growth some distance away from the interface. These points are illustrated graphically in Figs. 8 and 9 by comparing the hydrostatic stress distribution and void growth in front of a growing crack for a case $m = 1$ and $m = 1.5$. The results for the tensile specimen with $n = 0.1$. From Fig. 8 it can be seen that the hydrostatic stress in the case with $m = 1.5$ is higher than for the case with $m = 1$. In the mismatch case the highest hydrostatic stress will still be found at the interface. However, the zone of high hydrostatic stress extends further ahead of the current crack tip at positions shifted away from the interface compared to the case with $m = 1$. Fig. 9 compares the damage evolution for the two cases. Two important observations can be made. First, the void growth zone is more widespread in the mismatch case. Second, the zone of equal contours of void growth extends further ahead of the crack tip at distances away from the interface for $m = 1.5$, which can be linked to both the higher hydrostatic stresses and the lower constraint on the plastic deformation. McClintock [34] pointed out that a criterion for crack growth deviation in materials subject to plastic deformation should be linked to material softening first occurring at an angle to the initial crack plane. Such softening can be achieved due to the initially higher void growth rate away from the interface found for mismatch cases when using the GTN model. Hao et al. [28] coupled the GTN model with slip line analysis of a cracked mismatch specimen loaded in tension. Their analysis showed that softening, expressed through a reduction in the Mises stress, would happen along a 45° line to the interface, opening for crack growth deviation in this direction. Fig. 10(a) compares the distribution of the Mises stress in the two first layers of elements along the interface in the weak material, for a tensile specimen with mismatch $m = 1.25$ and $n = 0.05$. From this figure it can be seen that close to the crack tip the Mises stress in the element layer 2 falls below the level in layer 1 (layer 1 is the first element layer along the interface), indicating a stronger softening in the second element layer close to the crack tip. From Fig. 10(b), showing the crack growth path, it can be seen that this coincides with a shift in crack growth to the second element layer. Fig. 11(a) compares the Mises stress in the first two layers of elements for the same case as above, but with higher hardening, $n = 0.1$, at three different amounts of crack growth. It can be seen that initially the Mises stress in layer 1 lies below the level in layer 2. From Fig. 11(b), showing the crack growth path, the crack growth initially occurs in the first layer of elements. However, with further crack growth the Mises stress distribution in layers 1 and 2 becomes more equal, until after about 0.6 mm of crack growth, where the Mises stress in layer 2 falls below the level

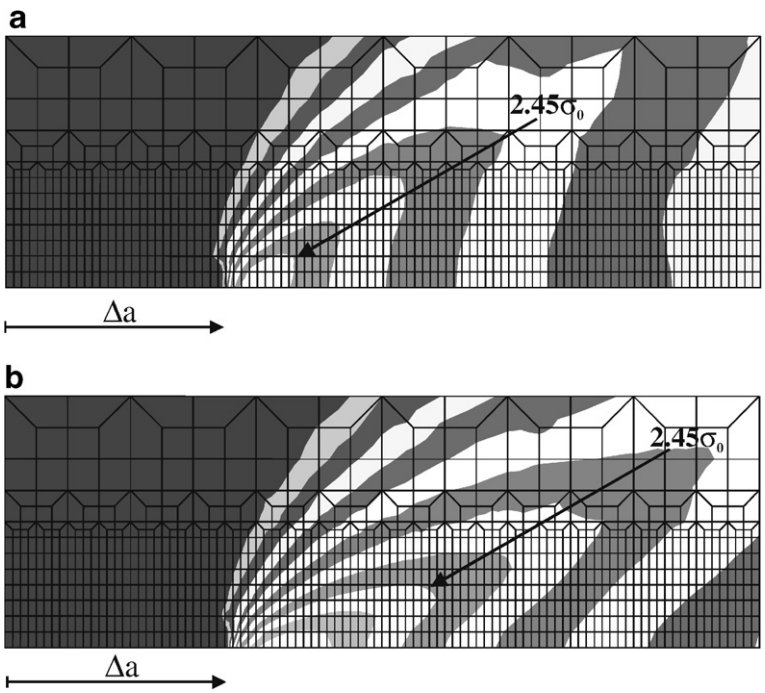

Fig. 8. Comparison of hydrostatic stress distribution for different mismatch levels after ca. 1.5 mm of crack growth. (a) $m = 1$. (b) $m = 1.5$. $n = 0.1$, tensile, $a/W = 0.15$.

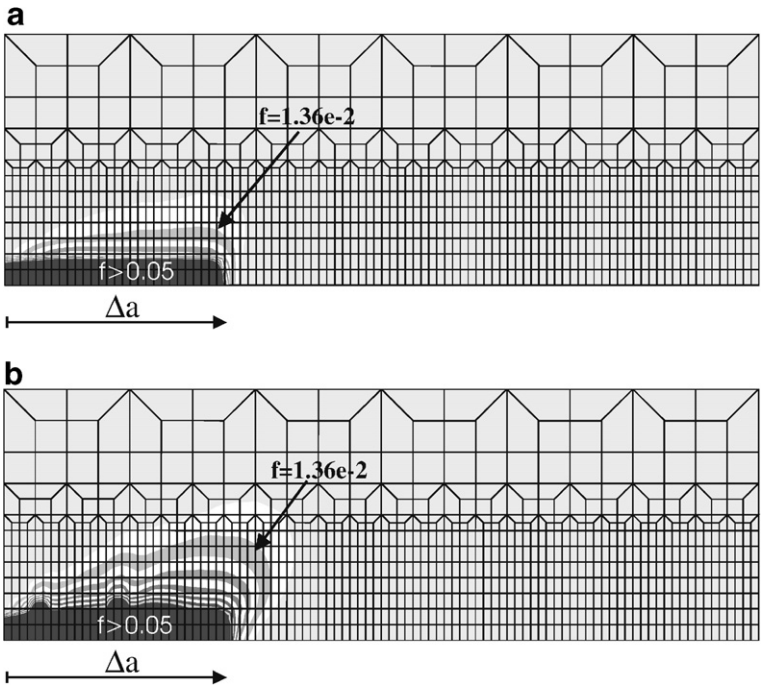

Fig. 9. Comparison of void volume fraction distribution for different mismatch levels after ca. 1.5 mm of crack growth. (a) $m = 1$. (b) $m = 1.5$. $n = 0.1$, tensile, $a/W = 0.15$.

in layer 1 close to the crack tip. From Fig. 11(b) it can be seen that this is the position where the crack growth shifts to element layer 2. These observations support McClintocks's proposed criterion for crack growth deviation.

4.4. Discussion on the effect of mismatch on ductile crack growth

From the results of the numerical simulations presented above it is indicated that the crack growth direction for the mismatch cases is mainly influenced by two factors, the hardening and the specimen geometry. The effect of hardening is linked to the local behaviour close to the crack tip. Increasing hardening elevates the stress field leading to preferred void growth close to the interface. Also, softening in the Gurson model is a competition between void growth and hardening. Higher hardening can more easily counteract the tendency for softening due to void growth, making softening in material layers away from the interface more difficult. Thus, increasing hardening will promote the tendency for the crack to grow along the interface. The influence of the geometry is related to the global deformation pattern in the specimen. The global plastic deformation will influence the stress/strain fields close to the crack tip under large scale plasticity, which will usually be the case for ductile crack growth in finite specimens. Fig. 12 shows the global slip line pattern for the shallow cracked tensile and the deep cracked bend specimens for perfectly plastic material. In the tensile specimen, the global plastic deformation will follow a line that is 45° to the initial crack plane. For the bend specimen the main deformation follows a circular pattern, with the slip lines emanating at an angle of 72° to the crack plane. The global deformation field will focus deformation in the direction of the major plastic flow. For the mismatch case, together with the increased plastic constraint at the interface, this will promote higher deformation-driven void growth at greater angles to the interface between the two materials. This effect will be stronger in the bend specimens compared to the tensile specimens.

Figs. 13 and 14 compare the crack growth direction for five different hardening levels for the tensile and bending specimens, respectively, for a mismatch level of $m = 1.25$. A mesh with a larger extension of the area of uniform element size in the normal direction to the interface was used for the bend specimen in these

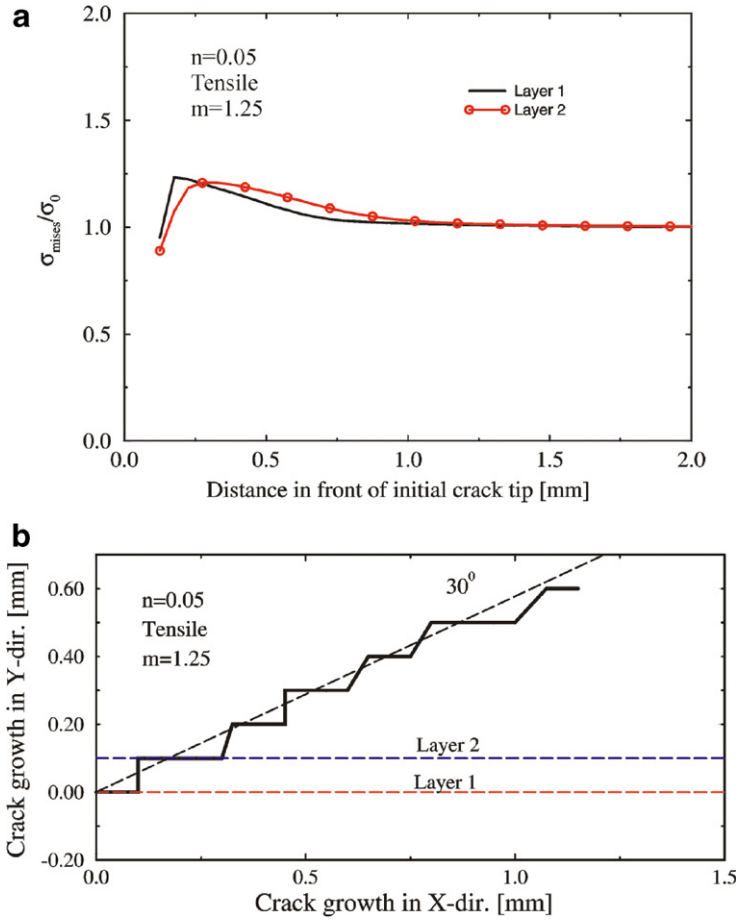

Fig. 10. (a) Comparison of Mises stress distribution ahead of the crack tip in the two first element layers in Mat 1. (b) Ductile crack growth path. Tensile loading, $a/W = 0.15$, $m = 1.25$, and $n = 0.05$.

analyses in order to track the crack growth for a longer distance for the hardening levels where significant deviation was observed. In both Figs. 13 and 14 a clear effect of hardening level is seen on the crack growth path. For the tensile specimen, Fig. 13, it can be seen that the crack path for the case with no hardening, $n = 0$, follows a 45° direction to the interface, in accordance with the global slip line field. As the hardening decreases the tendency for crack growth deviation decreases. In the case of the bending specimen, Fig. 14, the crack growth path tends to be "crooked", most markedly for the lower hardening levels, with an increasing tendency towards deviation as the crack moves further away from the interface. In the case with $n = 0$ the crack growth path displays slightly less deviation than the 72° slip line direction, mainly due to the "crooked" crack path with less tendency towards deviation for small amounts of crack growth. Also for the bending specimens the crack growth deviation increases for decreasing hardening. For a given hardening level it is observed that the tendency towards crack deviation is higher in the bend specimens compared to the tensile specimens.

In general the mismatch level has less influence on the crack growth path, compared to the importance of hardening and specimen geometry. However, one exception from this is found for the highest mismatch level, $m = 1.5$, in the case of bending for the hardening levels $n = 0.05$ and 0.1. In Fig. 10 it is seen that an initial part of about 0.5 mm crack growth is along the interface before deviation occurs for this mismatch level. The crack growth deviation is linked to a stronger tendency towards softening in material layers not at the interface. The bending case with $m = 1.5$ represents the situation with the highest hydrostatic stress level in all the analyses. This very high hydrostatic stress level gives rise to a strong softening effect in the material layer at the interface

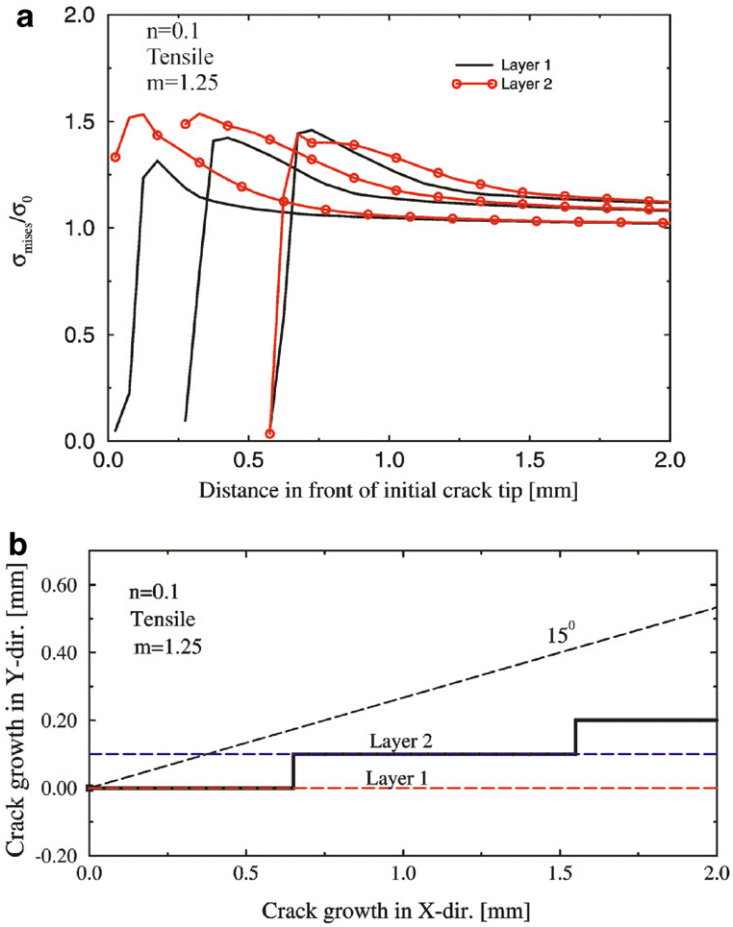

Fig. 11. (a) Comparison of Mises stress distribution ahead of the crack tip in the two first element layers in Mat 1, for increasing ductile crack growth. (b) Ductile crack growth path. Tensile loading, $a/W = 0.15$, $m = 1.25$, and $n = 0.1$.

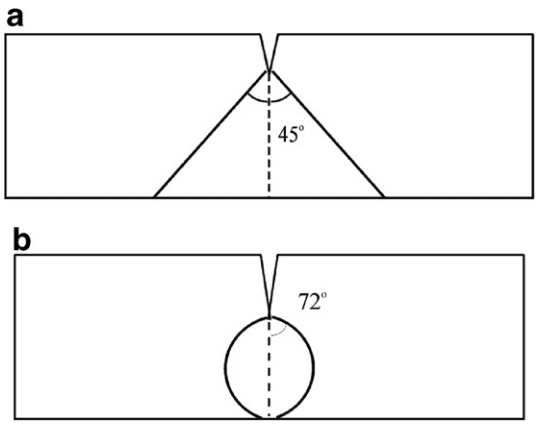

Fig. 12. Principal global plastic deformation/slip line patterns. (a) Specimen loaded in tension. (b) Specimen loaded in bending.

at some distance in front of the crack tip. Fig. 15 shows this effect where it can be seen that a drop in Mises stress is observed here. Because of this a very low initial resistance to crack growth is seen for the bend specimen with $m = 1.5$ in Fig. 11. In contrast to the deformation-driven crack deviation, which is strongly influenced by large

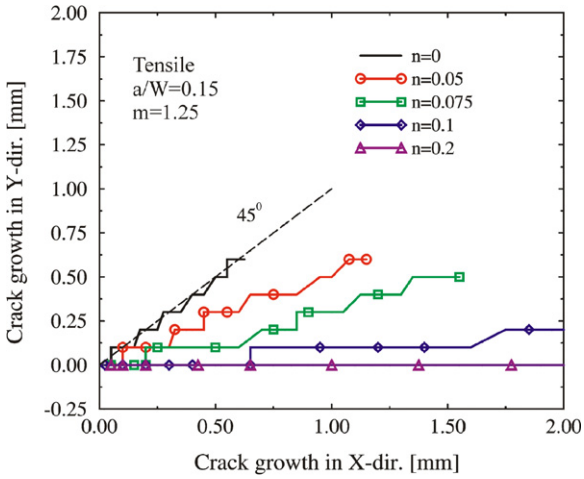

Fig. 13. Simulated crack growth paths for different levels of hardening for shallow cracked specimen loaded in tension with $m = 1.25$.

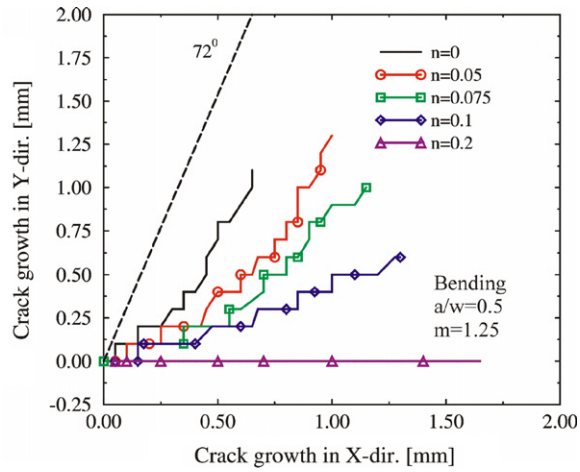

Fig. 14. Simulated crack growth paths for different levels of hardening for deep cracked specimen loaded in bending with $m = 1.25$.

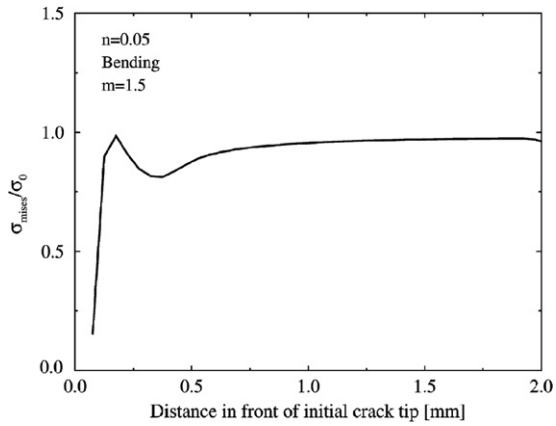

Fig. 15. Distribution of Mises stress ahead of the crack tip for deep cracked specimen loaded in bending with $m = 1.5$ and $n = 0.05$.

plastic deformation related to the global deformation, this latter effect is related to the exponential dependency of the stress triaxiality in the constitutive equation. Also, this phenomenon bears resemblance to cavitation observed ahead of the crack tip in constrained metal layers (see e.g. Tvergaard and Hutchinson [22]). Thus, for cases where very high hydrostatic stress levels due to mismatch are present at the interface, the simulations suggest that the crack growth path can be more influenced by the mismatch level.

The numerical simulations indicate that the effect of mismatch on the crack growth resistance is closely linked to the crack growth behaviour. For cracks growing along the interface mismatch will clearly reduce the $J - \Delta a$ curve, with increasing effect for increasing level of mismatch. In the analyses presented above this is the case for high hardening, $n = 0.2$, and high mismatch level, $m = 1.5$, for the tensile specimen with $n = 0.1$. In case of crack growth deviation away from the interface, the detrimental effect of mismatch on the crack growth resistance is reduced. Also, the relative effect of the mismatch level is reduced in case of crack deviation, mainly due to the reduced influence from the mismatch constraint at the interface. Further, due to the stronger tendency to crack deviation, the detrimental effect of mismatch relative to the homogeneous material will be lower in case of bending compared to tensile loading.

4.5. Mesh size dependence

As discussed in the introduction, the modelling of ductile crack growth usually displays significant mesh size dependence with regard to simulation of $J - \Delta a$ curves. For other parameters being held fixed,

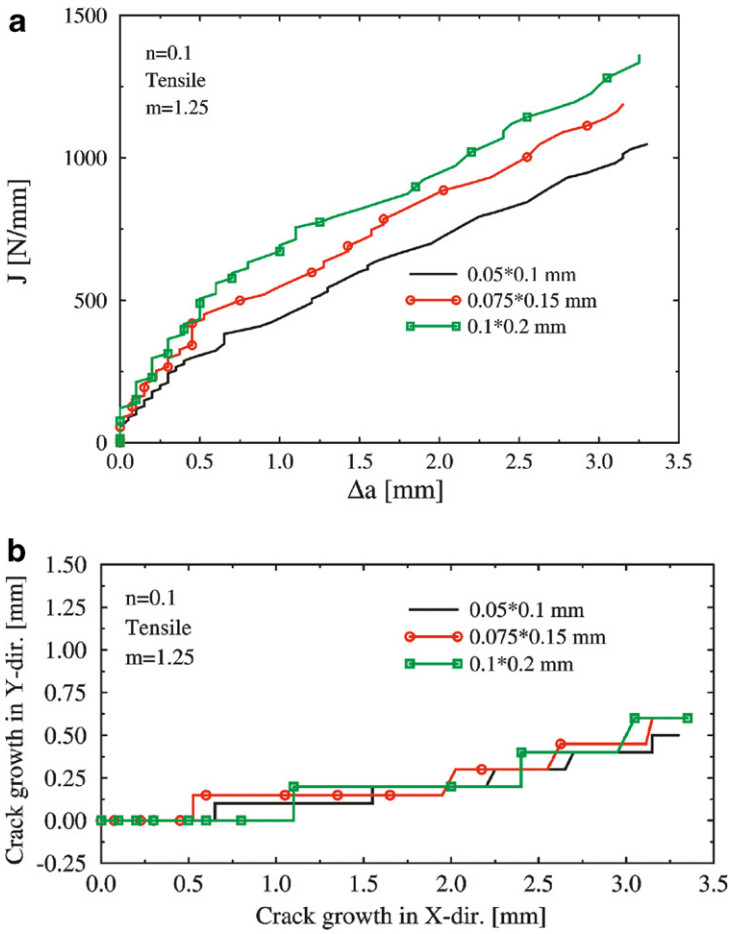

Fig. 16. Effect of mesh size on (a) and (c) $J - \Delta a$ curve and (b) and (d) crack growth path. (a) and (b) Shallow cracked specimen loaded in tension, (c) and (d) Deep cracked specimen loaded in bending, with $m = 1.25$ and $n = 0.1$.

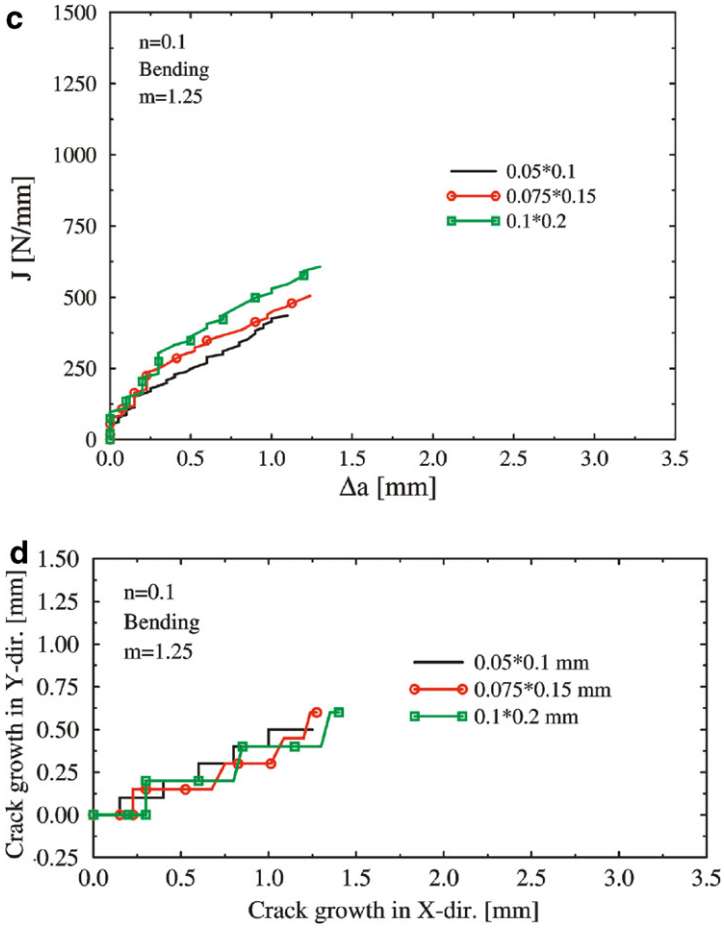

Fig. 16 (*continued*)

an increase in mesh size will elevate the crack growth resistance. In order to evaluate the effect of mesh size for the simulation of ductile crack growth we have compared three different element sizes. In addition to the element size $0.05 * 0.1$ mm used in the parametric study reported above, element sizes of $0.075 * 0.15$ and $0.1 * 0.2$ mm (maintaining the aspect ration of 2) are also applied. Fig. 16 compares the effect of mesh size for the bend and tensile specimen on the crack growth resistance and the crack growth path, for $m = 1.25$, $n = 0.1$ and $W = 50$ mm. An increase in mesh size increases the crack growth resistance, Fig. 16(a) and (c), while the crack growth paths are more or less independent of the element size. In line with other results in the literature, the crack growth resistance curves display an effect of the mesh size. However, as can be seen from Fig. 16(b) and (d), the crack growth deviation in the present work show only a weak dependency of the element size. A pronounced effect of mesh size was only observed in the extreme case of $m = 1.5$ and bending.

As discussed in Section 2, use of elements with initial square shape resulted in highly irregular stress fields in front of the crack tip. This mesh pattern tended to promote crack growth along the interface, with delayed deviation compared to cases with a mesh with aspect ratio equal to 2. This difference is mainly believed to be due to inappropriate representation of the stress field for the initially square shaped element pattern. It is underlined that the topology of the mesh pattern for the elements with aspect ratio equal to two did not only promote crack growth in certain directions, and the mesh pattern was able to simulate a wide range of crack growth paths.

5. Concluding remarks and discussion

2D plane strain FE analyses have been used to study of the effects of specimen size and mismatch on ductile crack growth in two different finite specimen geometries. The first geometry is a shallow cracked specimen ($a/W = 0.15$) loaded in tension, whereas the second geometry is a deep cracked specimen ($a/W = 0.5$) loaded in bending. With regard to the size effect on ductile crack growth resistance it is found that for small amounts of ductile crack growth the $J - \Delta a$ curves display little dependence on the specimen size, both for bend and tensile specimens. A more pronounced size effect is seen with further crack growth in the smallest specimens, and the size effect increases for decreasing hardening in the material. One difference is noted between the size effect for specimens loaded in tension and bending for low and intermediate hardening. For large amounts of crack growth in the former geometry the crack growth resistance is reduced in smaller specimens compared to larger ones, while the opposite is the case for bend specimens. This behaviour is explained by a different influence of the global deformation pattern in the remaining ligament in the two cases. Also, it is observed that the relative influence of the background plasticity is of greater importance for low hardening, contributing to a more pronounced size effect in the $J - \Delta a$ curves. The results above have been found through the use of a single assumption of the initial void volume fraction in the GTN model. Variation of this value could possibly have some influence on the relative effects reported here, but the main conclusions with regard to the effect of hardening and specimens size should remain the same, at least as long as fully plastic behaviour develops in the specimens.

For the yield stress mismatch cases, the analyses show that possible deviation of the crack growth path away from the interface appears as an important new parameter compared to the homogeneous case. It is found that the crack growth path is mainly influenced by two parameters, hardening and specimen geometry, for the mismatch levels and the material properties investigated. High material hardening will promote crack growth along the interface between the two materials. For lower hardening the influence of the global deformation in the specimen geometry becomes more important and increases the tendency towards crack deviation. In the limit of an elastic perfectly plastic matrix material the crack growth direction approaches the global slip line solution in the two geometries. In this respect it is observed that the tendency towards crack deviation is stronger in the bending specimens compared to the ones loaded in tension. In general, mismatch will decrease the crack growth resistance, and in cases where the crack grows along the interface the reduction in crack growth resistance clearly increases with increasing level of mismatch. However, when crack growth deviation occurs the detrimental effect of mismatch is reduced. These results are of interest concerning how crack growth resistance should be handled in structural assessment of welded structures with mismatch in material properties. One interesting aspect would be finding how to modify $J - \Delta a$ curves measured for homogeneous materials to take into account the effect of mismatch in such assessments. However, more work and verification against test results are needed before such scaling schemes will be available. Because hardening appears to be an important factor for the crack growth direction, sensitivity studies on which part of the hardening curve is the most important would be of interest. Another important issue is to what extent damage parameters fitted for a homogeneous material could be assumed to be representative also in the mismatch case. Here the spatial distribution of void initiating particles could be of greater importance. Although the results presented above do not display strong mesh size sensitivity for the crack growth path (except for the case discussed above, where high mismatch level leads to very high hydrostatic stresses at the interface), the mesh size will still influence the calculated resistance curve. In relation to this a clearer understanding of the influence of the different length scales involved in the fracture process would be of importance for further progress. The use of the GTN model with a given initial void volume fraction, as applied in the analyses above, is believed to capture the first order effect of hardening and specimen geometry on the crack growth direction. However, studies on the effect of including e.g. void nucleation terms would be of interest. With regard to crack growth deviation the criterion appears to be a stronger tendency to material softening at greater angles to the current crack growth direction. This will include some possible influence from the criterion used to predict coalescence. However, this dependency is probably small as long as coalescence will not occur at very small void volume fractions/local deformation levels. Additional analyses with different assumptions of the initial void volume fraction, not reported here, revealed little influence on the crack growth direction, and a better simulation of the softening behaviour in the material is probably of greater importance. On

the numerical side, improvements in the simulation of crack growth deviation can also be made. Some convergence problems were observed in the case of strong crack deviation. Inclusion of the element extinction techniques for the removal of elements in which coalescence has occurred could possibly reduce these problems.

Acknowledgement

The support from the Norwegian Research Council and Statoil, together with support from the ECSC/industry sponsored research project PRESS, for this work is highly acknowledged.

References

[1] McClintock FA. A criterion for ductile fracture by growth of holes. J Appl Mech 1968;(4):363–71.
[2] Rice JR, Tracey DM. On the ductile enlargement of voids in triaxial stress fields. J Mech Phys Solids 1969;17:201–17.
[3] Rice JR, Johnson ML. The role of large crack tip geometry changes in plane strain fracture. In: Kanninen MF et al., editors. Inelastic behaviour of solids. New York: McGraw-Hill; 1970. p. 641–72.
[4] Dugdale DS. Yielding of steel sheets containing slits. J Mech Phys Solids 1960;8:100–4.
[5] Barenblatt GI. The mathematical theory of equilibrium cracks in brittle fracture. Adv Appl Mech 1962;7:55–129.
[6] Tvergaard V, Hutchinson JW. The relation between crack growth resistance and fracture process parameters in elastic–plastic solids. J Mech Phys Solids 1992;40:1377–97.
[7] Tvergaard V, Hutchinson JW. Effect of T-stress on mode I crack growth resistance in a ductile solid. Int J Solids Struct 1994;31: 823–33.
[8] Tvergaard V, Hutchinson JW. Effect of strain dependent cohesive zone model on predictions of interface crack growth, EUROMECH – MECAMAT'96. 1st European Mechanics of Materials Conference on Local Approaches to Fracture, Journal De Physique IV, Colloque C6, supplément au Journal de Physique III, 1996, vol. 6: 165–72.
[9] Siegmund T, Brocks W. The role of cohesive strength and separation energy for modeling of ductile fracture. In: Paris PC, Jerina KL, editors. Fatigue and Fracture Mechanics: ASTM STP 1360, vol. 30. West Conshohocken, PA: American Society for Testing and Materials; 2000. p. 139–51.
[10] Siegmund T, Brocks W. A numerical study on the correlation between the work of separation and the dissipation rate in ductile fracture. Engng Fract Mech 2000;68:139–54.
[11] Gurson AL. Plastic flow and fracture of ductile materials incorporating void nucleation, growth and coalescence, PhD Thesis, Brown University, 1975.
[12] Rousselier G. Ductile fracture models and their potential in local approach of fracture. Nuclear Engng Design 1987;105:97–111.
[13] Xia L, Shih CF. Ductile crack growth – I. A numerical study using computational cells with microstructurally-based length scales. J Mech Phys Solids 1995;43:233–59.
[14] Xia L, Shih CF. Ductile crack growth – II. Void nucleation and geometry effects on macroscopic fracture behaviour. J Mech Phys Solids 1995;43:1953–81.
[15] Xia L, Shih CF, Hutchinson JW. A computational approach to ductile crack growth under large scale yielding conditions. J Mech Phys Solids 1995;43:389–413.
[16] Ruggieri C, Dodds RH. A transferability model for brittle fracture including constraint and ductile tearing effects: a probabilistic approach. Int J Fract 1996;79:309–40.
[17] Gao X, Shih CF, Tvergaard V, Needleman A. Constraint effects on the ductile-brittle transition in small scale yielding. J Mech Phys Solids 1996;44:1255–82.
[18] Zhang ZL, Thaulow C, Ødegård J. A complete Gurson model approach for ductile fracture. Engng Fract Mech 2000;67:155–68.
[19] Burstow MC, Howard IC. Predicting the effects of crack tip constraint on material resistance curves using ductile damage theory. Fatigue Fract Engng Mater Struct 1996;19:461–74.
[20] Siegmund T, Brocks W. Prediction of the work of separation and implications to modeling. Int J Fract 1999;99:97–116.
[21] Thaulow C, Hauge M, Zhang ZL, Ranestad Ø, Fattorini F. On the interrelationship between fracture toughness and material mismatch for cracks located at the fusion line of weldments. Engng Fract Mech 1999;64:367–82.
[22] Tvergaard V, Hutchinson JW. On the toughness of ductile adhesive joints. J Mech Phys Solids 1996;44:789–800.
[23] Lin G, Meng XG, Schwalbe KH. The effect of strength mis-match on mechanical performance of weld joints. Int J Fract 1999; 96:37–54.
[24] Xu X, Needleman A. Numerical simulations of fast crack growth in brittle solids. In J Mech Phys Solids 1994;42:1397–434.
[25] Scheider I. Simulation of cup-cone fracture in round bars using the cohesive zone model. In: Bathe KJ, editor. First M.I.T. Conferences on Computational Fluid and Solid Mechanics, vol. 1. Amsterdam: Elsevier; 2001. p. 460–2.
[26] Burstow MC, Howard IC. Damage mechanics models of ductile crack growth in welded specimens. Fatigue Fract Engng Mater Struct 2000;23:691–708.
[27] Moran PM, Shih CF. Crack growth and cleavage in mismatched welds: a micromechanics study using a cell model. Int J Fract 1998;92:153–74.

[28] Hao S, Brocks W, Kocak M, Schwalbe KH. On interface crack growth and the criterion to determine the direction of ductile crack propagation. In: Karihaloo BL, Mai YW, Ripley MI, Ritchie RO, editors. Advances in Fracture Research, 9th International Conference on Fracture, Sydney, 1997: p. 2627–34.
[29] Tvergaard V. Influence of voids on shear band instability under plane strain conditions. Int J Fract 1981;17:389–407.
[30] Tvergaard V. On localization in ductile materials containing spherical voids. Int J Fract 1982;18:237–52.
[31] Tvergaard V, Needleman A. Analysis of the cup-cone fracture in a round tensile bar. Acta Metall 1984;32:157–69.
[32] Thomason PF. Ductile fracture of metals. Oxford: Pergamon Press; 1990.
[33] Pardoen T, Hutchinson JW. An extended model for void growth and coalescence. J Mech Phys Solids 2000;48:2467–512.
[34] McClintock FA. Plasticity aspects of fracture. In: Liebowitz H, editor. Fracture, vol. 3. New York: Academic Press; 1971. p. 47–225.